Available online at www.sciencedirect.com

ScienceDirect

Underground Space 27 (2026) 45–57

www.keaipublishing.com/undsp

Research Paper

Numerical simulation on progressive leakage in shield tunnel and corresponding mitigation

Tianqi Zhang, Bangguo He, Zhitong Chen *, Gang Zheng, Chang Liu

School of Civil Engineering, Tianjin University, Tianjin 300072, China

Received 15 June 2025; received in revised form 21 September 2025; accepted 8 October 2025
Available online 7 January 2026

Abstract

Leakage disasters in shield tunnels frequently occur, leading to severe consequences such as tunnel collapse, road collapse, and building destruction. Since it is difficult to record the accident evolution process onsite, it is necessary to reproduce it through credible numerical simulations. However, traditional numerical methods face technical bottlenecks when simulating water–sand inrush in shield tunnels due to challenges such as large deformation analysis and fluid–structure coupling, making it difficult to simulate the process of disaster progression. To address this issue, a Coupled Eulerian–Lagrangian (CEL) method incorporating seepage analysis, referred to as the S-CEL method, was proposed to simulate the interaction between water, soil, and a shield tunnel during a disaster. A refined three-dimensional numerical model was developed using the S-CEL method to simulate the water–sand inrush process. The generation sequence of new leakage points at the segment joints and the mechanisms driving the progression of the disaster were revealed. New leakage points were progressively generated along the longitudinal direction of the tunnel. As the number of leakage rings increased, the amount of soil loss increased rapidly. This led to severe uneven settlement and dislocation deformation of the tunnel. A channel steel was introduced to reinforce the tunnel in the numerical simulation to mitigate or decelerate the progression of the leakage disaster. The connection method between the channel steel and tunnel segments was found to be pivotal to the strengthening effect. Employing only bolt anchoring showed limited efficacy, while enhancing the segment-steel interface with epoxy resin achieved much better performance in mitigating disaster progression.

Keywords: Leakage disaster; Water-sand inrush; Seepage Coupled Eulerian–Lagrangian (S-CEL); Shield tunnel; Channel steel; Reinforcement; Epoxy resin

1 Introduction

With the accelerated pace of urbanization and increasing exploitation of underground space resources, shield tunnels have seen a steady upward trend in deployment within urban rail transit and underground engineering projects. However, the dynamic interplay between complex geological formations and variable hydrological conditions presents persistent challenges regarding leakage risks throughout both the construction and operational phases (Zheng et al., 2024a, 2024b). Notable case studies demonstrate this issue. In 2003, Shanghai Metro Line 4 experienced a catastrophic water–sand inrush, leading to structural compromise of the tunnel, adjacent ground subsidence, subsequent tilting of overlying buildings, collapse of flood control walls, and piping failures (Bai et al., 2019; Tan et al., 2021). In 2016, a leakage in Tianjin Metro Line 1 severely damaged the tunnel segments, necessitating extensive repairs (Huang et al., 2020). In 2018, Foshan Metro Line 2 witnessed a water–sand inrush that triggered tunnel and roadway collapse, resulting in fatalities and injuries (Yu et al., 2020; Investigation Committee, 2018).

* Corresponding author.
E-mail address: chenzhitong1999@tju.edu.cn (Z. Chen).
Peer review under the responsibility of Tongji University

https://doi.org/10.1016/j.undsp.2025.10.006

In 2024, the leakage incident on Xi'an Metro Line 8 caused a large-scale ground collapse, destroying municipal utility pipelines. These incidents underscore the gravity of leakage-related catastrophes and highlight the pressing need for preventive strategies. Consequently, unravelling the evolutionary mechanisms of leakage disasters and establishing an effective prevention framework are imperative to ensure the safety and sustainability of underground infrastructure.

Numerous scholars have conducted extensive studies on leakage disasters in shield tunnels. The majority of existing experimental studies have employed reduced-scale models (Guan et al., 2022; Zheng et al., 2017, 2024d). However, their outcomes are largely limited to qualitative insights, and the quantitative responses of both soil and tunnel structures in practical engineering remain poorly understood. Given the significant challenges of fully replicating disaster progression through full-scale tests in practice, the development of robust numerical models for studying leakage disasters in shield tunnels has become indispensable.

In numerical studies, Meguid and Dang (2009) utilized the finite element method (FEM) to develop a circular cavity model and systematically analyzed the mechanism of soil erosion around tunnels. Liu et al. (2013) and Xu and Lu (2016) investigated the impact of local segment leakage on pore pressure, surface settlement, and tunnel deformation using numerical modelling. Zhang et al. (2017) constructed a tunnel-soil coupling model using the discrete element method (DEM) to elucidate the mechanical response mechanisms of seepage erosion in shield tunnels. Notably, existing numerical studies predominantly focus on structural deformation or soil loss induced by initial leakage. However, the complex process in which seepage erosion of soil triggers tunnel deformation and damage, which in turn exacerbates leakage, remains a challenge to simulate. This is primarily due to technical problems in large deformation simulations involving seepage analysis, which is a critical gap that necessitates urgent research.

The Coupled Eulerian–Lagrangian (CEL) method, which combines the advantages of Lagrangian and Eulerian meshes, excels in analyzing problems involving large deformations and structural failures (Cui et al., 2022; Kim, 2021). Consequently, it has been extensively used to simulate tunnel collapse and damage (Zheng et al., 2023b, 2024c). However, a critical limitation of the CEL is its inability to incorporate seepage effects; thus, it fails to account for water-soil-structure interactions and precludes the simulation of leakage disasters in shield tunnels. To bridge this gap, a novel numerical framework, termed the S-CEL method, was developed by integrating seepage analysis into the CEL framework. The enhanced approach successfully reproduced the evolution process of water–sand inrush in shield tunnels and addressed the mechanisms driving disaster progression in shield tunnels. Based on these insights, targeted reinforcement strategies were proposed to mitigate disasters, and their effects were quantitatively evaluated.

2 S-CEL method

2.1 Principle and framework

This study presents the CEL method incorporating seepage analysis, namely the S-CEL method, to simulate the development process of the water–sand inrush disasters in shield tunnels. In general, the simulation of this method involves the coupling of two types of analyses: CEL and seepage analysis (implemented in ABAQUS 2020). Data exchange (each explicit analysis step was performed 10 times) between the two analyses was performed using Python scripts (Python 2.7). As shown in Fig. 1, the execution steps of the S-CEL method are as follows.

Step 1: Initializing the model. In the model of seepage analysis (standard solver), the porosity, permeability coefficient, and pore pressure of the soil were initialized. In the CEL model (explicit solver), the soil and tunnel were modelled using Eulerian and Lagrangian meshes, respectively. The interaction between the soil and tunnel was simulated by general contact.

Step 2: Solving the seepage field. In the seepage analysis model, the initial leakage was activated, and the standard solver computed the seepage velocity field. Two core datasets were extracted: the pore pressure field (X, $\boldsymbol{P}_{\mathrm{w}}$) on the adjacent soil surface (X denoted three-dimensional coordinates, and $\boldsymbol{P}_{\mathrm{w}}$ denoted the corresponding pore pressure) and the soil seepage force distribution (I, $\boldsymbol{F}_{\mathrm{s}}$) ($I$ denoted the node number in the CEL model, and $\boldsymbol{F}_{\mathrm{s}}$ denoted the seepage force vector at that node).

Step 3: Solving tunnel deformation. Using a Python script, data import keywords were automatically inserted into the input file of the CEL analysis to accurately map the seepage field data from Step 2 to the corresponding nodes of the CEL model. Subsequently, the tunnel deformation and soil stress owing to the initial leakage were computed.

Step 4: Updating parameters. New leakage points were identified based on the tunnel deformation (both dislocations and openings at the joints after deformation were checked to determine the location of the new leakage points). By monitoring the Eulerian volume fraction (EVF), parameters such as the porosity and permeability coefficient of the soil were updated. Subsequently, the new parameters were fed back into the model of seepage analysis.

Step 5: Steps 2–4 were executed cyclically until the total elapsed time reached the preset simulation time, triggering the termination criterion and ending the simulation.

2.2 Validation

To validate the reliability of the S-CEL method in simulating water–sand inrush in shield tunnels, a model test of

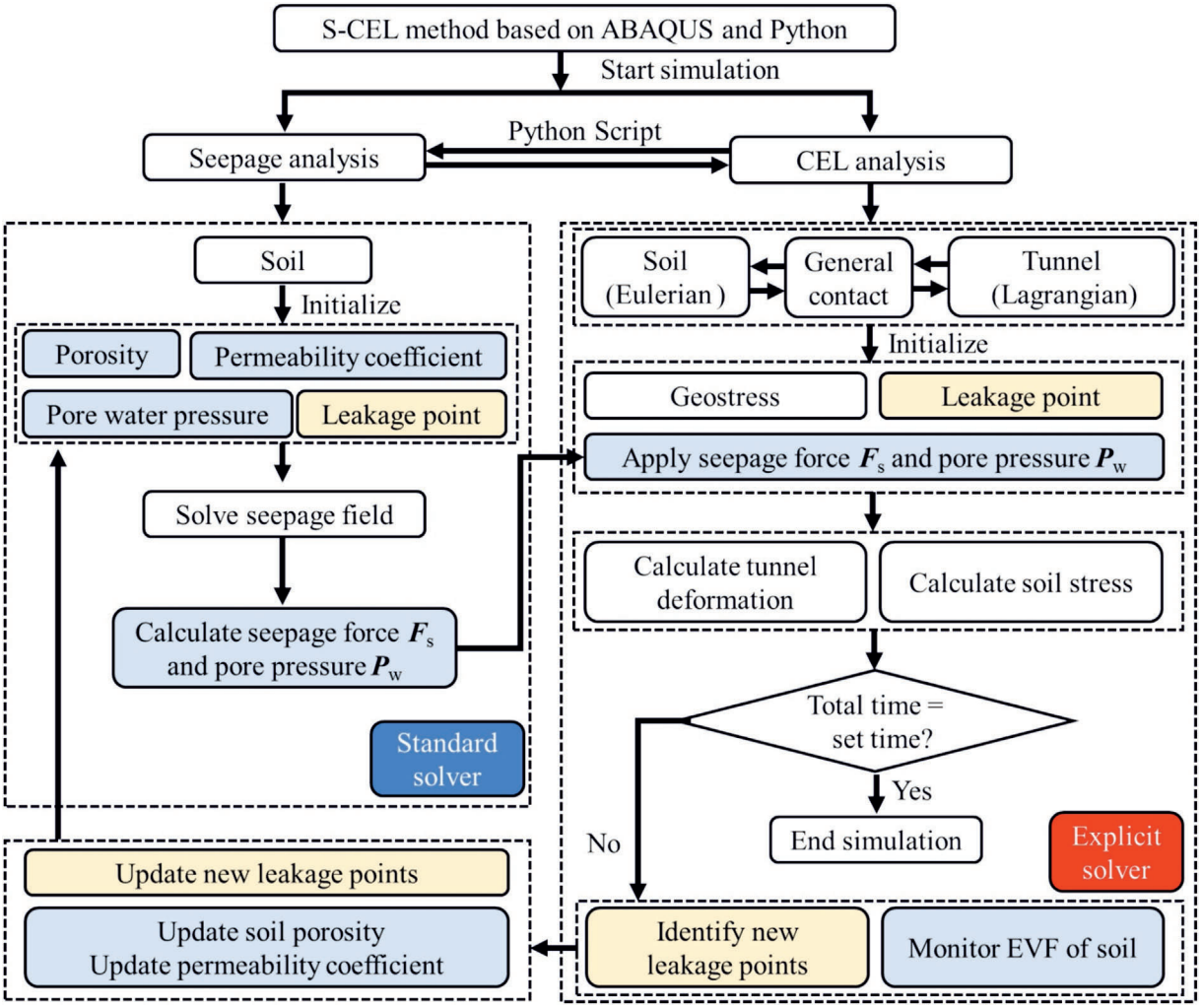

Fig. 1. Schematic of S-CEL method.

tunnel leakage performed by Zhang et al. (2022) was selected as the benchmark test. The test prescribed a cover depth (H_d) and a water level (h_w) of 300 mm, as shown in Fig. 2(a). The initial leakage was triggered at joint J1 (tunnel crown). Four coloured sand layers (L-1 to L-4) were preset in the model to visually present the subsurface settlements during tunnel leakage. Figure 2(b) shows the numerical reproduction model constructed using the S-CEL method.

Figure 2(c) shows a comparison between the experimental settlements and numerical predictions under the same volume loss of soil ($V_s = 342\ cm^3$). The results are in good agreement with the overall settlement and deformation patterns. The vertical displacement profiles demonstrate that the maximum settlement discrepancies across all layers are within 5%. This confirms that the S-CEL method can accurately capture the dynamic evolution of soil deformation patterns during a tunnel leakage, thereby establishing its applicability for simulating complex hydromechanical coupling processes in full-scale disasters. For more detailed validation of the S-CEL method, reference can be made to the research conducted by Zheng et al. (2025).

3 Numerical model

3.1 Model information

A three-dimensional numerical model was developed using the S-CEL method to simulate water–sand inrush in a full-scale shield tunnel. To improve computational efficiency, a half-symmetric model was built, with the $\alpha\beta\gamma$ plane defined as the symmetry plane (Fig. 3). The tunnel lining consisted of 25.5 rings, including 15.5 detailed rings (Rings #0 to #15, whose structural features were elaborately modelled) and 10 simplified rings (homogeneous circular rings). Each detailed ring comprised six segments: one key segment (K) with a central angle of 22.5°, and five standard segments (B1–B5), each with a central angle of 67.5°. The circumferential joint between Rings #i and #$(i + 1)$ was labeled CJ-i and further subdivided into CJ-i-1 to CJ-i-16, corresponding to 16 bolt positions. The six longitudinal joints between the adjacent segments in Ring #i were sequentially named LJ-i-1 to LJ-i-6. Straight bolts and a staggered-joint assembly scheme were used. The reinforcement configuration followed the design of typical

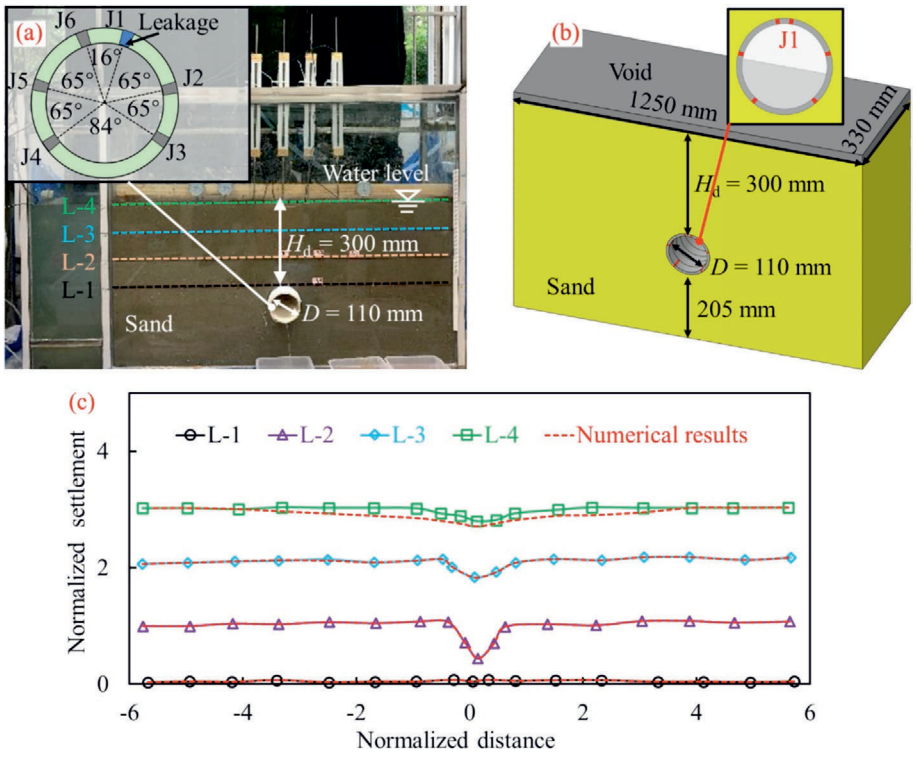

Fig. 2. Validation of S-CEL method. (a) Benchmark test (Zhang et al., 2022), (b) numerical model, and (c) result comparison.

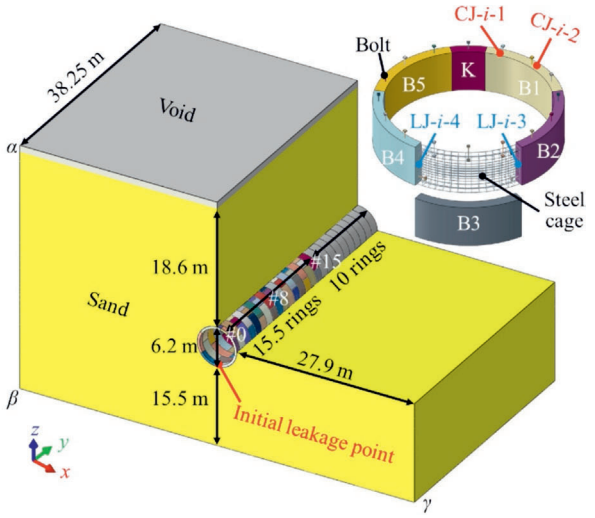

Fig. 3. S-CEL model.

Tianjin Metro tunnels: 10 external steel bars (16 mm diameter), 10 internal steel bars (20 mm diameter), and 10 mm diameter stirrups.

The tunnel lining had an outer diameter of 6.2 m, an inner diameter of 5.5 m, and a width of 1.5 m. The soil model measured 62.00 m (length, along the x-axis) × 38.2 5 m (width, along the y-axis) × 40.30 m (height, along the z-axis). A 1 m thick void layer was set at the top of the sand layer to prevent material spillage during the simulation. The tunnel was buried to a depth of 18.6 m, fully embedded within a 15.5 m thick sand stratum. The lateral boundaries, located 27.9 m from the tunnel walls (x-axis direction), ensured an adequate distance for the boundary condition implementation.

Normal displacements were constrained at the bottom and lateral boundaries of the model. For the soil-structure interaction, the normal contact between the tunnel and soil was specified as hard contact, with tangential behavior governed by the penalty function method (friction coefficient = 0.4) (Zheng et al., 2024c). Similarly, the segment-to-segment normal contact employed hard contact, and the tangential interaction followed the penalty method with a friction coefficient of 0.62 (Ye & Liu, 2021). To simulate bolts freely passing through the bolt holes, no contact or constraints were defined between the bolts and segments (Zhao et al., 2023). The initial leakage point was set at B3 in Ring 0. New leakage points were identified at the tunnel joints when the relative joint displacement (e.g., joint dislocation and opening) exceeded 12 mm (Zheng et al., 2018). To balance accuracy and efficiency, the leakage points identified in every one-tenth explicit analysis step were grouped into a single set for iterative calculations.

The model consisted of 1 880 732 nodes and 1 824 176 elements. The elements included 234 880 Eulerian hexahedral solid elements (EC3D8R) for the soil, 1 206 240 hexahedral solid elements (C3D8R) for the tunnel segments, 4102 beam elements (B31) for the bolts, and 248 340 truss elements (T3D2) for the steel bar.

3.2 Material parameters

The Mohr–Coulomb constitutive model was employed for the soil. The material parameters were determined according to Zheng et al. (2023a), as listed in Table 1. For the tunnel segment, the concrete damaged plasticity (CDP) model was adopted in accordance with the Code for Design of Concrete Structures (GB/T 50010—2010) (MOHURD, 2011), with its mechanical parameters (Zheng et al., 2023c; Wu et al., 2022) presented in Table 2. Both the steel bars and bolts utilized the bilinear material model, with their primary mechanical parameters (MOHURD, 2011) listed in Table 3.

To validate the reliability of the segment parameters, this study simulated the full-scale segmental lining loading test conducted by Liu et al. (2016), as shown in Fig. 4(a). The model test used 24 concentrated loads (P_1, P_2, P_3, etc.) to simulate the actual loads acting on the shield tunnel.

The loading path was divided into two stages, described as follows.

(1) First stage: Loads P_1, P_2, and P_3 increased linearly from zero. At the end of this stage, P_1 reached 300 kN, P_2 was 0.7 times P_1, and P_3 was 0.5 times the sum of P_1 and P_2 (i.e., $P_3 = 0.5(P_1 + P_2)$).
(2) Second stage: Load P_1 remained constant, P_2 decreased continuously until the structure reached its ultimate bearing capacity, and P_3 always maintained a value of $0.5(P_1 + P_2)$.

A comparison of the load-convergence deformation curves (Fig. 4(b)) showed that the deviations between the numerical results and test data were controlled within 10%, indicating that the model was able to simulate the mechanical behavior of full-scale tunnel structures.

4 Evolution mechanism of leakage disasters

Based on the S-CEL method proposed in Section 2 and the numerical model established in Section 3, this section discusses the simulation results of leakage disasters in shield tunnels.

Figure 5 illustrates the development process of the leakage disaster in the shield tunnel, which comprises initial and intensification stages. During the initial stage, the emergence of the initial leakage point led to a water–sand inrush. This disturbed the stratum around the tunnel, thereby leading to geostress redistribution and tunnel deformations (e.g., dislocations and openings). Once the relative joint displacement reached the limit of triggering leakage (12 mm in this study) (Zheng et al., 2018), more leakage points formed, indicating that the disaster had transitioned to the intensification stage. During this stage, a large amount of water–sand gushed into the tunnel through the new leakage points, which resulted in a significant expansion of the disturbed stratum zone, further aggravating tunnel deformation and damage. This process repeatedly and progressively caused an increasing number of tunnel linings to suffer deformation, damage, and leakage, thereby driving the continuous progression of the disaster.

Figure 6 shows the evolution sequence and spatial distribution of the new leakage points. Obviously, new leakage points emerged progressively along the longitudinal direction of the tunnel in a ring-by-ring manner. The 2nd group of leakage points (②) first appeared at the circumferential joint #0 (CJ-0-8 and CJ-0-9), just adjacent to the initial leakage point. Subsequently, the development of the disaster accelerated markedly; starting from the 3rd group (③), the number of leakage points increased rapidly.

New leakage points predominantly arose at the circumferential joints, which accounted for approximately 93% of all leakage points, whereas the longitudinal joints contributed only 7% (marked with a red square), which was a negligible proportion. This distinct pattern highlighted the dominant role of longitudinal deformations (uneven settlements and dislocations) over transverse deformations (diameter convergence) in the tunnel.

5 Countermeasures against leakage disasters

The findings presented in Section 4 revealed that approximately 93% of the leakage points arose at the circumferential joints, indicating insufficient stiffness (Liu & Sun, 2020; Lin et al., 2020). This structural deficiency predisposes the joints to relative displacement (e.g., dislocations and openings), which progressively results in new

Table 2
Parameters of segment concrete.

ρ (kg/m^3)	E (GPa)	v	ϕ (°)	ϵ	f_{b0}/f_{c0}	K_c	μ
2400	35.50	0.2	38	0.1	1.16	0.6667	0.0005

Note: ϕ-Dilation angle, ϵ-Flow potential eccentricity, f_{b0}/f_{c0}-Biaxial/uniaxial compression plastic strain ratio, K_c-Invariant stress ratio, and μ-Viscosity.

Table 1
Parameters of soil.

ρ (kg/m^3)	E (kPa)	v	φ (°)	c (kPa)	k (m/s)	e
1660	62 400	0.3	31.725	13.8375	5.787×10^{-5}	0.603

Note: ρ-Density, E-Young's modulus, v-Poisson's ratio, φ-Friction angle, c-Cohesion, k-Permeability coefficient, and e-Void ratio.

Table 3
Parameters of rebar and bolt.

Materials	ρ (kg/m^3)	E (GPa)	v	Yield strength (MPa)	Ultimate strength (MPa)
HPB335	7800	206	0.3	335	455
HRB400	7800	206	0.3	400	540
Bolt	7800	210	0.3	400	500

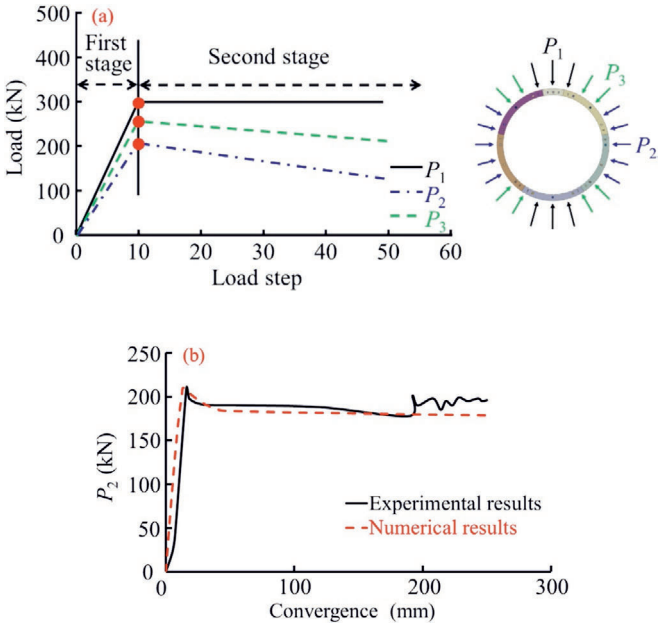

Fig. 4. Validation of segment parameters. (a) Loading scheme (Liu et al., 2016), and (b) comparison of tunnel responses.

leakage. Enhancing the inter-ring connections can potentially mitigate or decelerate the progression of leakage disasters. To test the feasibility of this concept, a longitudinal channel steel was used to strengthen the tunnel. A systematic analysis was conducted to evaluate the inhibitory effects of various bracing configurations on the propagation of leakage, with particular attention on their capacity to constrain joint deformation during disasters.

5.1 Configurations of longitudinal channel steel

As shown in Fig. 7, the channel steel selected was type 20b, as specified in Hot rolled section steel (GB/T 706—2016) (Masteel Group Holding, 2016), with a strength grade of Q355B (parameters listed in Table 4 (Angang Steel Company Limited, 2018)). Its height was $h = 200$ mm, leg width was $b = 75$ mm, web thickness was $t_w = 9$ mm, and flange thickness was $t = 11$ mm. In the cross-section of the tunnel, a total of six channel steels were arranged, numbered No. 1 to No. 6, respectively. Each channel steel had a length of 23.25 m, which was consistent with the length of the detailed rings.

In this study, three cases were analyzed. Case 1 served as the control group in which no reinforcement was adopted. In Case 2, the channel steel was connected to the segments via anchoring. Each channel steel had only one anchor point on each segment ring. In Case 3, in addition to anchoring, a layer of epoxy resin was applied at the interface between the channel steels and segments for bonding, further enhancing the connection between them.

To accurately simulate the interface slip, failure, and separation between the channel steels and concrete in Case 3, a bilinear cohesive zone model (CZM) was employed to simulate the bonding effect of the epoxy resin. The model accounted for the mechanical behavior of the epoxy resin interface under combined tension and shear. As shown in Fig. 8, as the interface deformation progressed, the mechanical behavior evolved in three distinct stages.

Stage i was the elastic stage. The cohesive stress increased linearly with the relative displacement until the initial damage threshold was reached.

Stage ii was the softening stage. After reaching its peak value, the cohesive stress gradually decreased to zero as the displacement increased.

Stage iii was the debonding stage. The relative displacement continued to increase, whereas the cohesive stress remained zero.

The specific parameters were determined following Sun et al. (2022); such parameter settings have been widely recognized and applied in relevant studies (Li et al., 2023; Liu et al., 2025). For tensile strength: $\sigma_{max,n} = 2.4$ MPa, $s_{max,n} = 0.8$ mm, and $G_n^c = 960$ N/m. For shear strength: $\sigma_{max,t} = 2.5$ MPa, $s_{max,t} = 4.5$ mm, and $G_t^c = 5625$ N/m. The normal stiffness (K_n) was 144 MPa/mm, and the tangential stiffness (K_t) was 40 MPa/mm.

5.2 Strengthening effect

Figure 9 shows the tunnel settlements under different soil mass losses for the three cases. Notably, enhancing the interface bonding strength between the tunnel lining and channel steel using epoxy resin significantly improved the capacity of the inter-ring joints to resist discontinuous deformation. By contrast, bolt anchoring between the segments and channel steel exhibited limited effectiveness in mitigating settlement. For instance, under the mass loss of soil $M = 2.03$ t (purple line), Case 1 (without any reinforcement) recorded a maximum settlement of 39.6 mm. Case 2, in which bolt anchoring was used to connect the channel steel and the segments, reduced the maximum settlement to 33.3 mm. In comparison, Case 3, with the

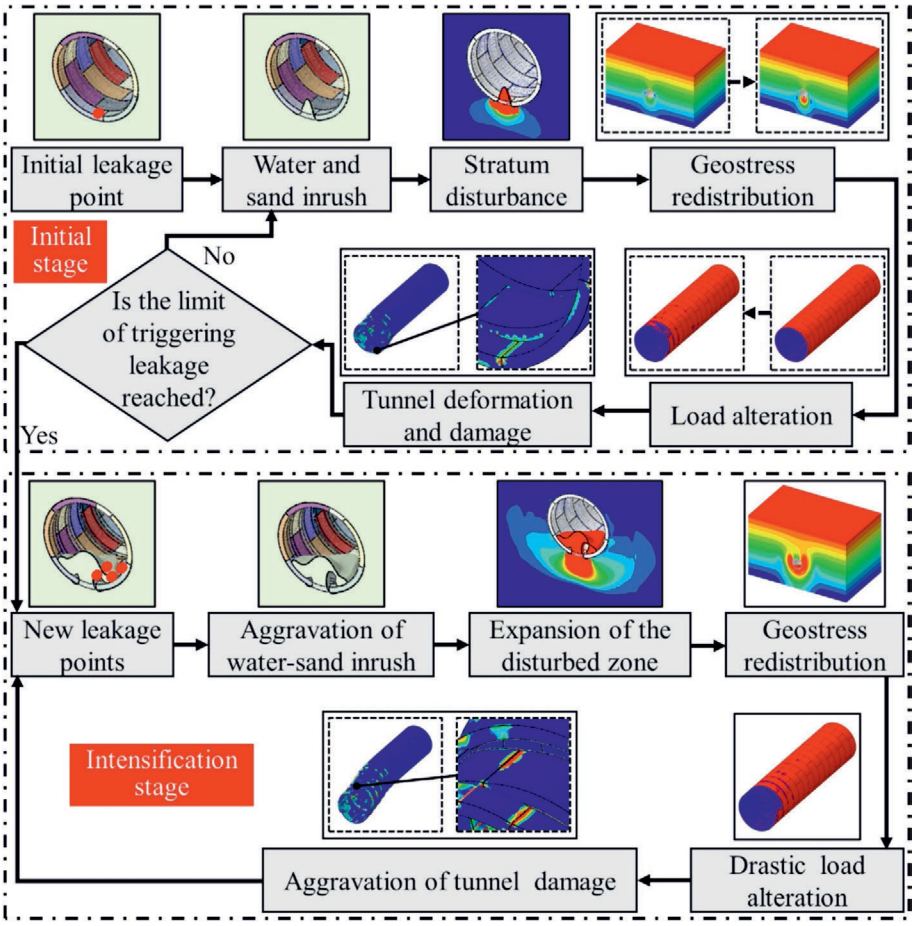

Fig. 5. Development process of leakage disasters in shield tunnel (reproduced by numerical simulation).

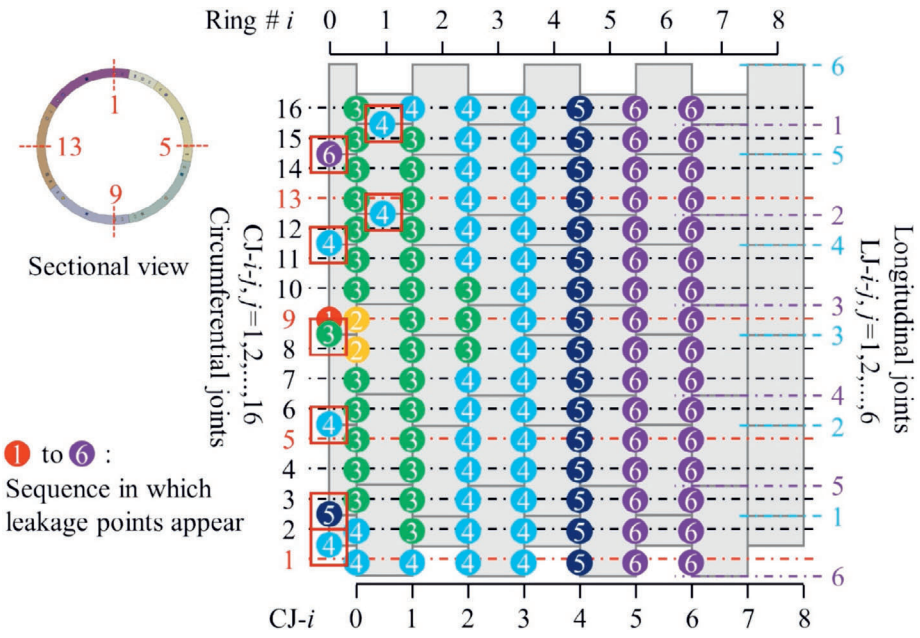

Fig. 6. Evolution sequence and spatial distribution of new leakage points.

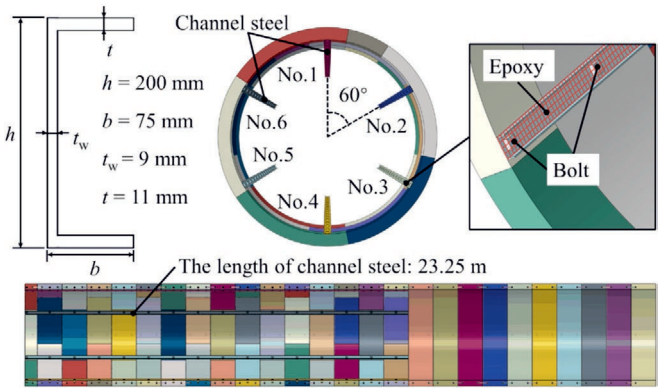

Fig. 7. Layout of channel steels.

additional application of epoxy resin bonding, achieved a significantly lower maximum settlement of only 22.4 mm.

Further analysis revealed distinct deformation patterns. In Cases 1 and 2, settlement developed sequentially starting from Ring #0, with the 2nd group of leakage points occurring at the joint between Rings #0 and #1. By contrast, Case 3 exhibited an integral settlement of Rings #0 to #3 with the 2nd group of leakage points appearing at the joint between Rings #3 and #4. This divergence indicated that the epoxy-enhanced connections significantly improved the structural integrity of the tunnel by enabling a more uniform deformation distribution across adjacent rings.

As shown in Fig. 10, the Von Mises stress distributions in the channel steels are presented under the mass loss condition of soil $M = 3.2$ t. In Case 2, only the No. 4 channel steel exhibited significantly high stress values, whereas the other five channel steels exhibited relatively low stress levels. This phenomenon was primarily owing to the substantial segmental lining deformation (uneven settlement) occurring at the tunnel invert, where the initial leakage occurred. As the No. 4 channel steel was located at the tunnel bottom, it directly bore the shear loads induced by the joint dislocations. By contrast, all six channel steels in Case 3 demonstrated notably elevated stress distributions. This behavior can be linked to the introduction of an epoxy bonding interface between the channel steels and segments. The enhanced interfacial connection facilitated a more integrated structural response, enabling synergistic deformation between the channel steels and tunnel linings. Consequently, this configuration optimized the shear resistance capacity of the channel steels by ensuring a more uniform stress distribution and full utilization of their mechanical properties.

To further quantify the health status of the leakage shield tunnels in the 3 cases, an evaluation method for the health status of the tunnel-soil system was proposed. The specific procedure is as follows.

Step 1: Grade classification of the indicator. Four indicators (MOHURD, 2013) were employed in the evaluation method, i.e., joint dislocation (d, mm), joint opening (o, mm), convergence deformation (c, ‰D), and surface settlement (s, mm). Among the four indicators, the joint dislocation and opening reflected the integrity and sealing performance of the tunnel structure. The convergence deformation characterized the overall deformation trend and stability of the tunnel. The surface settlement indicated the degree of soil loss and environmental disturbance. Each indicator was divided into four grades. The four grades ranged from grade I (safest) to grade IV (most dangerous).

Step 2: Indicator scoring. Scores were assigned to the four graded indicators. Two scoring metrics, t_r and t_i, were introduced. For grades I to IV, the t_r scores were assigned as 1, 2, 3, and 4, respectively, while the t_i scores were assigned as 0, 0.1, 0.3, and 0.5, respectively (Tongji University & China Construction, 2020).

Table 4
Parameters of channel steel (Angang Steel Company Limited, 2018).

Materials	ρ (kg/m^3)	E (GPa)	v	Yield strength (MPa)	Ultimate strength (MPa)
Q355B	7850	206	0.3	355	455

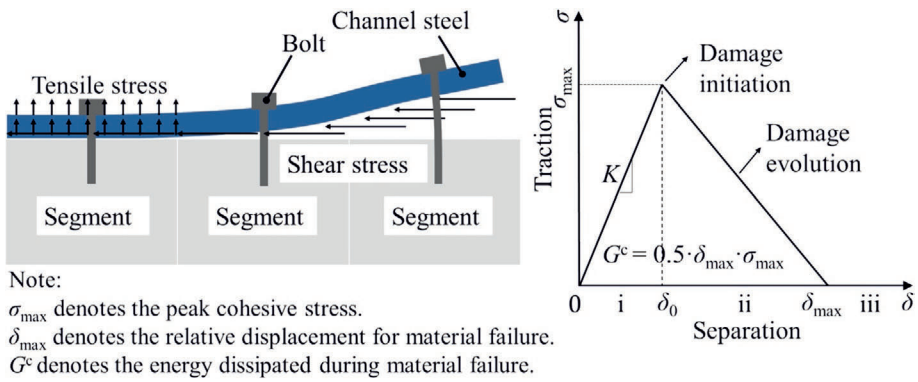

Fig. 8. CZM model for epoxy resin interface.

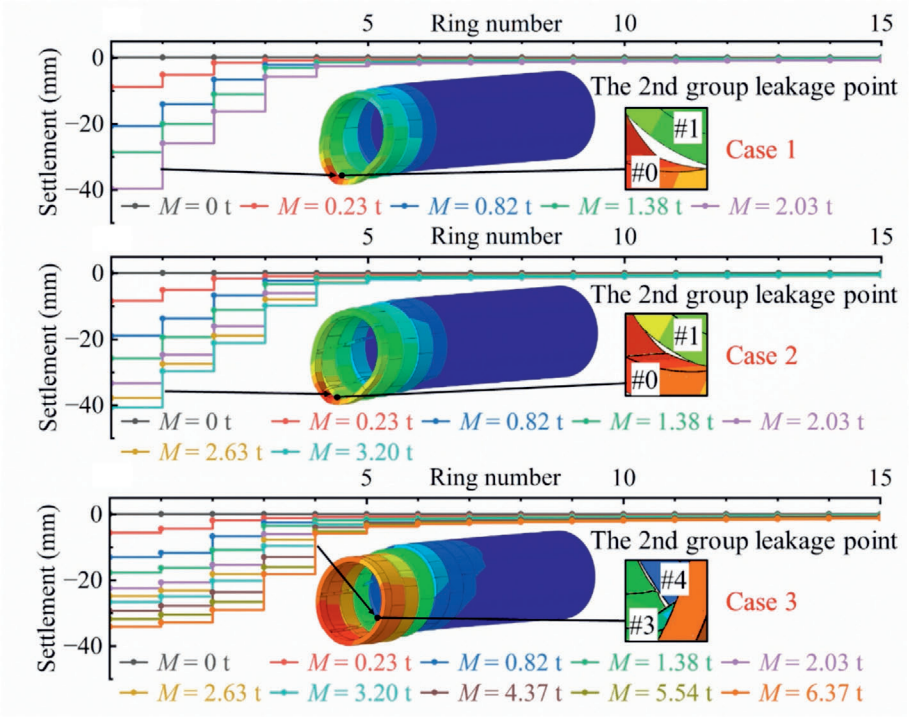

Fig. 9. Tunnel settlements under different mass loss of soil M.

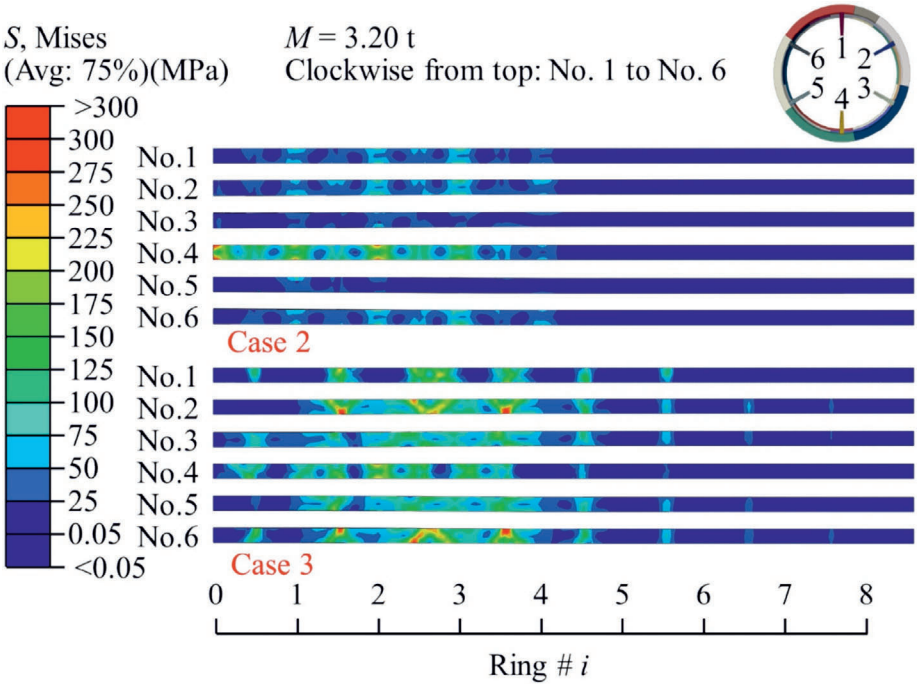

Fig. 10. Von Mises stress contours of channel steels.

Step 3: Health status evaluation of single-segment ring. The health status of the single-segment ring was evaluated using the H_S and defined as

$$H_S = 5.5 - \left(t_{max} + \sum_{i=0, i \neq j}^{4} t_i \right), \quad (1)$$

where t_{max} was the maximum value of the t_r scores among the four indicators, and $\sum_{i=1,i\neq j}^{4} t_i$ represented the summation of the t_i scores of the remaining three indicators (the t_r score of the jth indicator was the maximum among all four evaluated indicators). Based on the H_S values, the health grades of a single-segment ring can be classified into

four categories: A, B, C, and D. The classification criteria are illustrated in Fig. 11.

Step 4: Health status evaluation of the tunnel interval. The health index for a tunnel interval (H_T) was derived by summing the H_S values of individual segment rings calculated using Eq. (1). Thus, the overall health status of the tunnel interval can be evaluated quantitatively.

Figure 12 shows the decline in H_T as the leakage disaster progresses in all three cases. Five typical moments were selected for the analysis, corresponding to the numbers of leakage rings of 0, 2, 4, 6, and 8. Among the four indicators, surface settlement and joint dislocation had the most significant impacts on tunnel health, whereas the effects of joint opening and convergence deformation were relatively less significant. This indicates that during the progression of leakage disasters, the longitudinal uneven deformation of the tunnel and mass loss of the soil are the two key contributing factors. In addition, the development of the disaster also exhibited obvious nonlinear characteristics; the overall tunnel health index H_T initially decreased slowly, but with the generation of new leakage points, a notable drop in H_T occurred. In particular, after the number of leakage rings reached 6, a large number of segment rings degraded to health grade D.

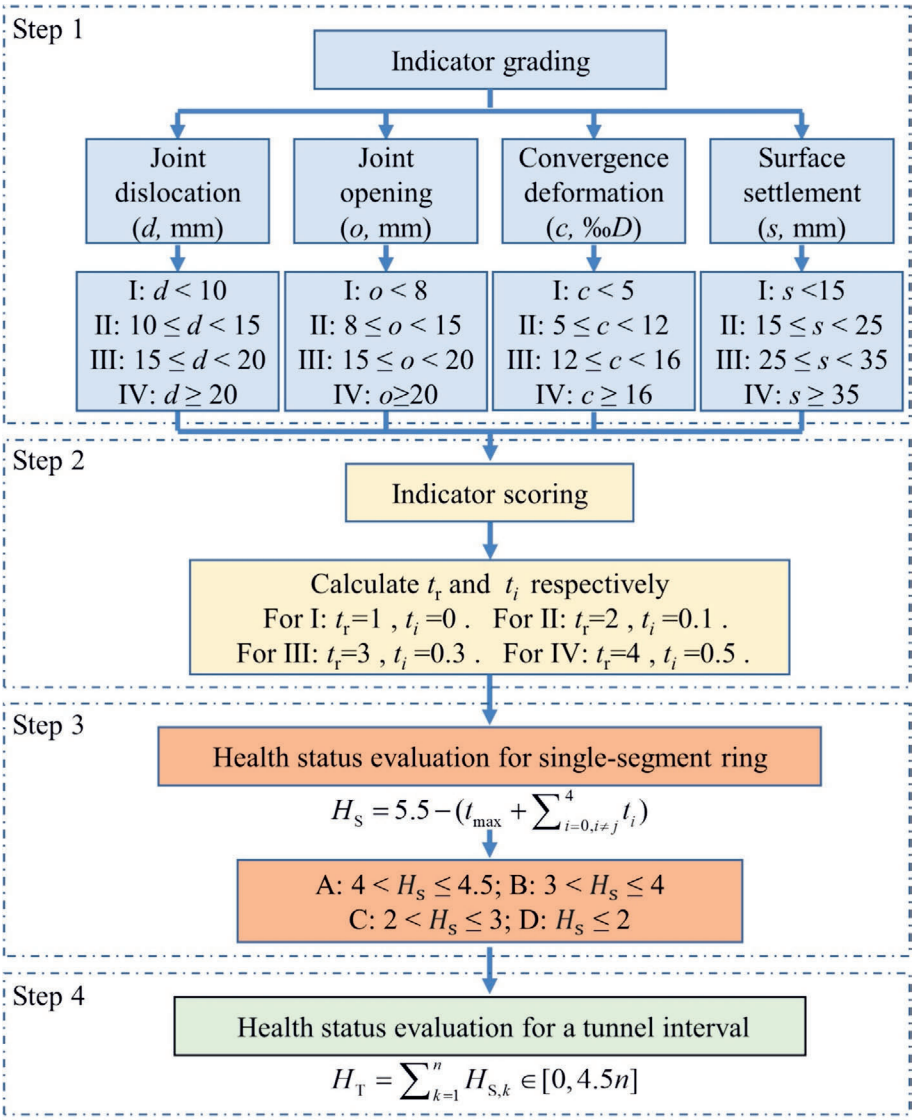

Note :
1. H_S : health index of a single segment ring.
2. H_T : health index of a tunnel interval.
3. n : the total number of segment rings in the evaluation interval.

Fig. 11. Evaluation procedures of tunnel health status.

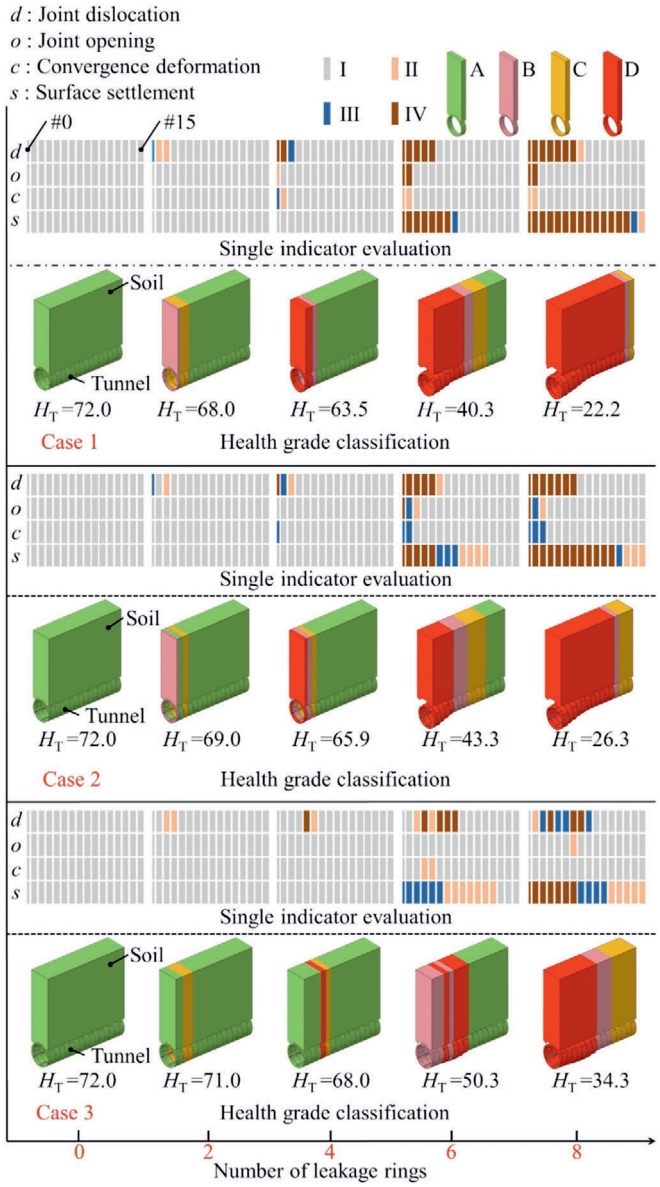

Fig. 12. Evaluating health status of shield tunnels as leakage disasters progressed.

With the same number of leakage rings, using only bolt anchoring to connect the channel steel and segmental rings had limited effectiveness in mitigating the decline in H_T. For instance, when the number of leakage rings reached 8, 14 segment rings were classified as health grade D, one ring as grade C, and one ring as grade B in Case 1. Case 2 (bolt anchoring only) yielded 12 grade D rings, one grade C ring, and 3 grade B rings, demonstrating only a 14.29% reduction in grade D segmental rings compared to Case 1. By contrast, integrating epoxy resin to strengthen the interface between the channel steel and segmental rings significantly inhibited H_T degradation. Under the same conditions, Case 3 (epoxy-enhanced connection) recorded 8 grade D rings, 3 grade C rings, and 5 grade B rings, achieving a 42.86% reduction in grade D segmental rings relative to Case 1.

6 Conclusions

In this study, the CEL method incorporating seepage analysis was presented to simulate the development process of water–sand inrush disasters in shield tunnels. The process of generating new leakage points in the shield tunnel as the disaster progressed was revealed. A channel steel reinforcement method was proposed as a countermeasure against disasters, and its effectiveness in mitigating them was evaluated. The main conclusions are summarized as follows.

(1) The development process of a leakage disaster in a shield tunnel comprised initial and intensification stages. During the intensification stage, a large amount of water–sand gushed into the tunnel through the new leakage points, which resulted in a significant expansion of the disturbed stratum zone, further aggravating tunnel deformation and damage.
(2) Approximately 93% of the leakage points occurred at the circumferential joints during the disaster, indicating insufficient stiffness. This structural deficiency predisposed the joints to relative displacement (e.g., dislocations and openings), which progressively resulted in new leakage. Enhancing the inter-ring connection, e.g., employing channel steel to reinforce the tunnel, can mitigate or decelerate the progression of leakage disasters.
(3) The connection method between the channel steel and tunnel segments was pivotal to the strengthening effect. Bolt anchoring alone showed limited efficacy in mitigating disaster progression, whereas enhancing the interface between the channel steels and segments with epoxy resin enabled more integrated structural behavior, facilitating synergistic deformation between the channel steels and tunnel linings. Consequently, this configuration significantly optimized the shear resistance of the channel steels by ensuring uniform stress distribution and full utilization of their mechanical properties.
(4) A comprehensive method was proposed to evaluate the health status of the tunnel-soil system. It can be used to quantify the severity of disasters in a leakage shield tunnel or assess the effectiveness of reinforcement measures.

To focus on the primary leakage mechanisms and associated countermeasures, the modelling in this study was based on a single sand layer, with no consideration given to the presence of multi-layered strata (e.g., clay layers). Subsequent research should incorporate such scenarios and perform parameter analyses.

Data availability

The data that support the findings of this study are available from the corresponding author upon reasonable request.

CRediT authorship contribution statement

Tianqi Zhang: Project administration, Conceptualization. **Bangguo He:** Writing – original draft, Software. **Zhitong Chen:** Supervision, Methodology, Data curation. **Gang Zheng:** Supervision, Methodology. **Chang Liu:** Visualization, Supervision.

Declaration of competing interest

The authors declare that they have no known competing financial interests or personal relationships that could have appeared to influence the work reported in this paper.

Acknowledgement

The authors would like to acknowledge the financial support from the National Natural Science Foundation of China (Grant Nos. 52478408 and 52278406) and the Innovative Research Group Project of the National Natural Science Foundation of China (Grant No. 52421005).

References

Angang Steel Company Limited (2018). Administration of Quality Supervision Inspection and Quarantine. *GB/T 1591—2018: High strength low alloy structural steels*. Standard Press of China, Beijing, China (in Chinese).

Bai, Y., Hu, X. D., & Xiao, X. C. (2019). *Major underground engineering accidents at home and abroad and repair technology* (2nd ed.). China Architecture & Building Press (in Chinese).

Cui, Q., Zhang, L. L., Chen, X. Y., Cao, Z. J., Wei, X., Zhang, J., Xu, J. B., Liu, D. S., & Du, C. L. (2022). Quantitative risk assessment of landslides with direct simulation of pre-failure to post-failure behaviors. *Acta Geotechnica, 17*(10), 4497–4514.

Guan, F., Wei, D. Q., Lei, J. S., Shi, Y. F., & Cao, C. W. (2022). Experimental study on lining response of metro shield tunnel under the influence of ground cavity. *Journal of Railway Science and Engineering, 19*(2), 461–469 (in Chinese).

Huang, L. C., Ma, J. J., Lei, M. F., Liu, L. H., Lin, Y. X., & Zhang, Z. Y. (2020). Soil-water inrush induced shield tunnel lining damage and its stabilization: A case study. *Tunnelling and Underground Space Technology, 97*, 103290.

Investigation Committee (2018). Investigation report on "2.7" water leakage and ground collapse major accident in Project I of Foshan Metro Line 2 in Guangdong, the people's Government of Guangdong Province of China (in Chinese).

Kim, D. (2021). Large deformation finite element analyses in TBM tunnel excavation: CEL and auto-remeshing approach. *Tunnelling and Underground Space Technology, 116*, 104081.

Li, Z., Liu, X. Z., Lai, H. R., Yang, Z. L., & Wang, B. Z. (2023). Detailed damage mechanism of deformed shield tunnel linings reinforced by steel plates. *Engineering Failure Analysis, 143*, 106850.

Lin, Z. J., Liu, S. M., & Wang, J. C. (2020). Longitudinal reinforcement effect of shield tunnel segments in soft soil. *Journal of Ground Improvement, 2*(6), 478–482.

Liu, X., & Sun, Q. H. (2020). Case analysis on progressive collapse of shield tunnel linings. *Hazard Control in Tunnelling and Underground Engineering, 2*(2), 21–30 (in Chinese).

Liu, X., Bai, Y., Yuan, Y., & Mang, H. A. (2016). Experimental investigation of the ultimate bearing capacity of continuously jointed segmental tunnel linings. *Structure and Infrastructure Engineering, 12*(10), 1364–1379.

Liu, X., Hong, J. Y., & Liu, Z. (2025). Investigations on mechanical behavior of longitudinal joints in segmental tunnel linings reinforced with epoxy bonded-bolted steel plates. *Tunnelling and Underground Space Technology, 163*, 106724.

Liu, Y., Zhang, D. M., & Huang, H. M. (2013). Influence of long-term partial drainage of shield tunnel on tunnel deformation and surface settlement. *Rock and Soil Mechanics, 34*(1), 290–298.

Masteel (Group) Holding Co., Ltd. (2016). *GB/T 706—2016: Hot rolled section steel*. Standard Press of China, Beijing, China (in Chinese).

Meguid, M. A., & Dang, H. K. (2009). The effect of erosion voids on existing tunnel linings. *Tunnelling and Underground Space Technology, 24*(3), 278–286.

Ministry of Housing and Urban-Rural Development of the People's Republic of China. (2011). *GB 50010—2010: Code for design of concrete structures*. China Building Industry Press, Beijing, China (in Chinese).

Ministry of Housing and Urban-Rural Development of the People's Republic of China. (2013). *GB 50911—2013: Code for monitoring measurement of urban rail transit engineering*. China Architecture & Building Press, Beijing, China. (in Chinese).

Sun, Y. Z., Yu, Y., Wang, J. C., Ye, Y. L., & Tan, Q. Y. (2022). Mechanical properties of linings of shield tunnel strengthened by steel plates considering interface effects. *Chinese Journal of Geotechnical Engineering, 44*(2), 343–351 (in Chinese).

Tan, Y., Lu, Y., & Wang, D. L. (2021). Catastrophic failure of Shanghai metro line 4 in July, 2003: Occurrence, emergency response, and disaster relief. *Journal of Performance of Constructed Facilities, 35*(1), 04020125.

Tongji University, & China Construction Engineering Industry Technology Research Institute Co., Ltd. (2020). *T/CECS 788—2020: Technical specification for inspection of shield tunnel structures disease in urban rail transit*. China Architecture & Building Press, Beijing, China (in Chinese).

Wu, H. N., Chen, S., Chen, R. P., Cheng, H. Z., & Feng, D. L. (2022). Deformation behaviors and failure mechanism of segmental RC lining under unloading condition. *Tunnelling and Underground Space Technology, 130*, 104687.

Xu, G. W., & Lu, D. Y. (2016). Mechanical behavior of shield tunnel considering nonlinearity of flexural rigidity and leakage of joints. *Chinese Journal of Geotechnical Engineering, 38*(7), 1202–1211 (in Chinese).

Ye, Z., & Liu, H. B. (2021). Investigating the relationship between erosion-induced structural damage and lining displacement parameters in shield tunnelling. *Computers and Geotechnics, 133*, 104041.

Yu, C., Zhou, A. N., Chen, J., Arulrajah, A., & Horpibulsuk, S. (2020). Analysis of a tunnel failure caused by leakage of the shield tail seal system. *Underground Space, 5*(2), 105–114.

Zhang, D. M., Gao, C. P., Yin, Z. Y., Wang, R. L., & Yang, T. L. (2017). Particle flow simulation of seepage erosion around shield tunnel. *Rock and Soil Mechanics, 38*(S1), 429–438.

Zhang, Z. G., Mao, M. D., Pan, Y. T., Zhang, M. X., Ma, S. K., Cheng, Z. X., & Wu, Z. T. (2022). Experimental study for joint leakage process of tunnel lining and particle flow numerical simulation. *Engineering Failure Analysis, 138*, 106348.

Zhao, D. B., Huang, Y. T., Chen, X. S., Han, K. H., Chen, C., Zhao, X. F., & Chen, W. T. (2023). Numerical investigations on dynamic responses of subway segmental tunnel lining structures under internal blasts. *Tunnelling and Underground Space Technology, 135*, 105058.

Zheng, G., Chen, Z. T., Zhang, T. Q., Qiu, H. M., Wang, K., & Diao, Y. (2024a). Particle-scale study on backward erosion of multilayer erodible medium under converging flow: Experimental tests and numerical modelling. *Acta Geotechnica, 19*(10), 7075–7087.

Zheng, G., Chen, Z. T., Zhang, T. Q., Wang, K., & Diao, Y. (2024b). Experimental study on the erosion morphology of fine sand under converging flow considering the impact of soil effective stress. *Acta Geotechnica, 19*(2), 1129–1135.

Zheng, G., Cui, T., Cheng, X. S., Diao, Y., Zhang, T. Q., Sun, J. B., & Ge, L. B. (2017). Study of the collapse mechanism of shield tunnels due to the failure of segments in sandy ground. *Engineering Failure Analysis, 79*, 464–490.

Zheng, G., Qiu, H. M., Zhang, T. Q., Chen, Z. T., & Liu, M. S. (2025). Mechanism of water and sand inrush in shield tunnel based on CEL method integrating seepage analysis. *Chinese Journal of Geotechnical Engineering*, 1–13 (in Chinese).

Zheng, G., Qiu, H. M., Zhang, T. Q., Sun, J. B., Cheng, H. Y., & Diao, Y. (2024c). Zheng induced by developing contact loss. *Engineering Failure Analysis, 155*, 107748.

Zheng, G., Qiu, H. M., Zhang, T. Q., Wang, T., Sun, J. B., Cui, T., & Diao, Y. (2024d). Experimental study of the effects of contact loss under a shield tunnel invert. *Acta Geotechnica, 19*(6), 4189–4199.

Zheng, G., Sun, J. B., Zhang, T. Q., Zhang, X. K., Cheng, H. Y., Wang, H., & Diao, Y. (2023a). Mechanism and countermeasures of progressive failure in shield tunnels. *Tunnelling and Underground Space Technology, 131*, 104797.

Zheng, G., Sun, J. B., Zhang, T. Q., Zhang, X. K., Li, X., Cheng, H. Y., Bai, N., & Diao, Y. (2023b). Numerical study on the impact of local failure on adjacent structures in a shield tunnel. *Acta Geotechnica, 18* (4), 2155–2168.

Zheng, G., Yao, J., Dai, X., Yang, X. Y., & Sun, J. Y. (2018). Experimental study on sand inflow under different opening widths of shield tunnel segments. *Chinese Journal of Geotechnical Engineering, 40* (6), 969–977 (in Chinese).

Zheng, G., Zhang, X. K., Zhang, T. Q., Sun, J. B., Qiu, H. M., & Diao, Y. (2023c). Numerical study on mechanical behavior and ultimate bearing capacity of shield segment joints under different load conditions. *Tunnelling and Underground Space Technology, 139*, 105204.